Adhesion of Nanoparticles to Vesicles: A Brownian Dynamics Simulation

Hiroshi Noguchi and Masako Takasu
Department of Applied Molecular Science, Institute for Molecular Science, Okazaki 444-8585, Japan

ABSTRACT We studied the interaction of bilayer vesicles and adhesive nanoparticles using a Brownian dynamics simulation. The nanoparticles are simple models of proteins or colloids. The adhering nanoparticle induces the morphological change of the vesicle: budding, formation of two vesicles in which only outer monolayers are connected, and fission. We also show that the nanoparticle promotes the fusion process: fusion-pore opening from a stalk intermediate, a neck-like structure that only connects outer monolayers of two vesicles. The nanoparticle bends the stalk, and induces the pore opening.

INTRODUCTION

In living cells, fission and fusion events frequently occur in various processes, such as endo- or exocytosis, protein trafficking, fertilization, and viral infection (Lipowsky and Sackmann, 1995; Jahn and Südhof, 1999; Allan and Balch, 1999). The studies of their mechanisms are biologically important. Budding, fission, and fusion of lipid vesicles have been extensively studied for simple model systems.

The many morphologies of vesicles are understood by the coarse-grained surface models where the bilayer membrane is treated as a smooth continuous surface (Lipowsky and Sackmann, 1995; Hotani et al., 1999; Kumar et al., 2001). However, in these models, the artificial recombination of surfaces is needed to investigate the shape transformations with topological change such as fission (Chen et al., 1997). It is not possible to apply these methods to the dynamics of the structural change of membranes. In contrast, some authors studied lipid bilayer structures using molecular dynamics (MD) (Pastor, 1994; Tieleman et al., 1997; Lindahl and Edholm, 2000; Saiz and Klein, 2001; Ohta-Iino et al., 2001). It has only been applied for a small number of molecules and short time dynamics because of limited computational resources.

Some mesoscopic models between atomic and macroscopic resolutions have been applied to surfactant/water mixtures and block copolymer systems: coarse-grained molecular simulations (Bernardes, 1996; Goetz et al., 1999), self-consistent theory (Netz and Schick, 1996; Li and Schick 2000; Kawakatsu 1997; van Vlimmeren et al., 1999), and dissipative particle dynamics (DPD) (Groot et al., 1999; Groot and Rabone, 2001). Particularly, DPD is a powerful method taking into account hydrodynamic interactions. The self-assembly into vesicles is simulated by lattice Monte Carlo method (Bernardes, 1996) and DPD (Yamamoto et al., 2002).

Recently, we proposed another simple model of amphiphilic molecules to investigate the shape transformations with topological change with molecular resolution (Noguchi and Takasu, 2001a). We used three-dimensional Brownian dynamics. An amphiphilic molecule is modeled as a rigid rod. Solvent molecules are not taken into account explicitly, and "hydrophobic" interaction is mimicked by the multibody local density potential of the hydrophobic segments. The amphiphilic molecules self-assemble into vesicles with bilayer structures. We also clarified two pathways of spontaneous vesicle fusion (Noguchi and Takasu, 2001b). This model does not include hydrodynamic interactions and allows the volume change of a vesicle. The long-ranged hydrodynamic interactions can accelerate the structural changes (Groot et al., 1999; Maurits et al., 1998), and this effect is estimated using scaling argument for a budding dynamics (Kumar et al., 2001). The volume constraint should decelerate the various structural changes. However, the absence of solvent molecules reduces computational time, and enables the model to be applied to the phenomena, largely changing the size of the molecular aggregate. We simulated the structural changes of a pulled vesicle (Noguchi and Takasu, 2002). The pulled vesicle stretches and forms a dumbbell-like structure, where two vesicles connect a long cylindrical structure. At a certain force, it becomes 20 times longer than the initial vesicle in 1 ms.

In our present paper, we added a spherical nanoparticle interacting attractively with the hydrophilic segments of amphiphilic molecules. We investigate the budding and fission of a vesicle induced by the adhesion of the nanoparticle. This is a simple model system of phagocytosis, and should also provide basic information to transfer drug-carrier complexes (Woodle and Scaria 2001; Angelova and Tsoneva 1999). The adhesion is usually caused by specific binding of ligands to membrane receptors or by electrostatic interactions. The cationic colloids or small vesicles adhere to anionic large vesicles or cells and vice versa (Chenevier et al., 2000; Huebner et al., 1999). Dietrich et al. (1997) investigated the adhesion of sulfate Latex spheres to neutral-lipid vesicles. However, the capture mechanisms with

Submitted August 20, 2001 and accepted for publication March 5, 2002.

Address reprint requests to Dr. Hiroshi Noguchi, Dept. of Applied Molecular Science, Institute for Molecular Science, Okazaki 444-8585, Japan. Tel.: +81-564-55-7257; Fax: +81-564-54-2254; E-mail: noguchi@ims.ac.jp.

Dr. Takasu's present address is Depart. of Computational Science, Kanazawa Univ., Kakuma Kanazawa 920-1192, Japan.

0006-3495/02/07/299/10 $2.00

molecular resolution are unresolved. One purpose of the present paper is to examine the basic capture mechanisms. We also clarify that the nanoparticle mimics the fusion protein, and promotes the fusion process of two vesicles.

METHOD

An amphiphilic molecule is modeled as one hydrophilic segment ($j = 1$) and two hydrophobic segments ($j = 2, 3$), which are separated by a fixed distance σ and are fixed on a line. Thus, this model explicitly takes into account the translational and orientational degree of freedom for phospholipid molecules with two hydrophobic tails and ignores the intra-chain degrees of freedom including *trans-gauche* transformation. A nanoparticle is modeled as a sphere with radius r_{np}. The interaction between amphiphilic molecules ($i = 1, \ldots, N$) is given by a repulsive soft-core potential U_{REP} and an attractive "hydrophobic" potential U_{HP}: $U_{AM} = U_{REP} + U_{HP}$.

Both segments have the same soft radius r_{am},

$$U_{REP} = \sum_{i \neq i'} U_{rep}(2r_{am}, |\mathbf{r}_{ij} - \mathbf{r}_{i'j'}|), \quad (1)$$

$$U_{rep}(r_0, r) = \exp\{-20(r - r_0)/\sigma\} \quad (2)$$

The hydrophobic objects assemble not by a direct attraction, but by the repulsion with water molecules. Because solvent molecules are not taken into account explicitly, this hydrophobic interaction is mimicked by the function $U_{hp}(\rho)$ of the local unnormalized density of hydrophobic segments,

$$\rho_{i,j} = \sum_{i \neq i', j'=2,3} h(|\mathbf{r}_{ij} - \mathbf{r}_{i'j'}|),$$

with weighting function,

$$h(r) = \frac{1}{\exp\{20(r/\sigma - 1.9)\} + 1}.$$

$\rho_{i,j}$ is the number of hydrophobic segments in the sphere whose radius is $\sim 1.9\sigma$. If a radius larger than 2σ is chosen, the density of a middle segment $\rho_{i,2}$ counts hydrophobic segments at the back of the hydrophilic segment $r_{i,1}$. Thus, we chose the radius of 1.9σ. U_{HP} is given by

$$U_{HP} = \sum_{j=2,3} U_{hp}(\rho_{i,j}),$$

$$U_{hp}(\rho) = \begin{cases} -0.5\rho & \rho < \rho^* - 1 \\ 0.25(\rho - \rho^*)^2 - c & \rho^* - 1 \le \rho < \rho^* \\ -c & \rho^* \le \rho. \end{cases} \quad (3)$$

We used the values $\rho^* = 10$ and $c = 4.75$ at $j = 2$, and $\rho^* = 14$ and $c = 6.75$ at $j = 3$. The values of c are given by $c = 0.5\rho^* - 0.25$ to connect the potential continuously at $\rho = \rho^* - 1$. The harmonic potential at $\rho^* - 1 \le \rho < \rho^*$ is used to reduce the force from $0.5\, d\rho_{i,j}/d\mathbf{r}_{i,j}$ to 0 continuously. At low density ($\rho < \rho^* - 1$), $U_{hp}(\rho)$ acts as the pair-wise potential $-h(r)$. We assume that the segment is shielded by hydrophobic segments from solvent molecules and hydrophilic segments at ρ^*. Thus, $U_{hp}(\rho)$ is constant at higher density ($\rho \ge \rho^*$). We modified the usual pair-wise potential with cutoff at high density ρ^*. If the pair-wise potential $-h(r)$ is used instead of $U_{hp}(\rho)$, the bilayer membrane has no fluid phase and does not form a vesicle spontaneously.

The nanoparticle interacts with amphiphilic molecules by potential U_{NP}:

$$U_{NP} = \sum_{j=2,3} U_{rep}(r_{am} + r_{np}, |\mathbf{r}_{ij} - \mathbf{r}_{np}|) + \sum U_{adh}(r_{am} + r_{np}, |\mathbf{r}_{i1} - \mathbf{r}_{np}|) \quad (4)$$

We used the same type of repulsive potential as that between amphiphilic molecules. The nanoparticle only attracts hydrophilic segments of amphiphilic molecules. $U_{adh}(r_0, r)$ is given by

$$U_{adh}(r_0, r) = \varepsilon_{np}\left[\exp\left\{\frac{20(r - r_0)}{\sigma}\right\} - \frac{1}{\exp\{20(r - r_0 - 0.6\sigma)/\sigma\} + 1}\right], \quad (5)$$

where ε_{np} is the depth of $U_{adh}(r_0, r)$. The adhesion potential $U_{adh}(r_0, r)$ is short-range potential, and the well width of this potential is $\sim 0.6\sigma$. When the bilayer membrane interacts with the nanoparticle, the nanoparticle attracts the hydrophilic segments only in proximal monolayer. To simplify the model, we used not an electrostatic potential but the potential, which has similar shape to $U_{rep}(r)$ and $h(r)$.

The motion of the segments of the molecule and the nanoparticle follows the underdamped Langevin equation,

$$m\frac{d^2\mathbf{r}_{i,j}}{dt^2} = -\zeta\frac{d\mathbf{r}_{i,j}}{dt} + \mathbf{g}_{i,j}(t) - \frac{\partial U}{\partial \mathbf{r}_{i,j}}, \quad (6)$$

$$m_{np}\frac{d^2\mathbf{r}_{np}}{dt^2} = -\zeta_{np}\frac{d\mathbf{r}_{np}}{dt} + \mathbf{g}_{np}(t) - \frac{\partial U}{\partial \mathbf{r}_{np}}, \quad (7)$$

where m (m_{np}) is the mass and ζ (ζ_{np}) is the friction constant of the segments of the molecule (the nanoparticle), and $U = U_{AM} + U_{NP}$. $\mathbf{g}_{i,j}(t)$ and $\mathbf{g}_{np}(t)$ are Gaussian white noise and obey the fluctuation-dissipation theorem. The equations of the translational and rotational motions of amphiphilic molecules are integrated by a leapfrog algorithm with a time step of $\Delta t = 0.01$ (Allen and Tildesley, 1987).

We cut off $U_{rep}(r_0, r)$ at $r_0 + 0.3\sigma$ and $U_{adh}(r_0, r)$ at $r_0 + 0.9\sigma$. We set $h(r) = 1$ for $r < 1.6\sigma$ and $h(r) = 0$ for $r \ge 2.2\sigma$. We used the periodic boundary condition with the cubic box with the side length 50 or 100σ. We fixed the segment radius $r_{am} = 0.5\sigma$, the segment mass $m = 1$, the friction constant of segments $\zeta = 1$, and the temperature $T = 0.2$ (We set k_B to unity hereafter). The radius of the nanoparticle is changed: $r_{np} = \sigma, 2\sigma$, and 3σ. The mass and friction constant of the nanoparticle are the same values for the translational motion of amphiphilic molecules: $m_{np} = 3$ and $\zeta_{np} = 3$. We present our results with the reduced units, $\sigma = 1$. In the budding simulation, we changed the depth of $U_{adh}(r_0, r)$: $\varepsilon_{np} = 0.5, 1, 2, 3, 4$ at $N = 2000$ and $\varepsilon_{np} = 0.05, 0.1, 0.25, 0.5, 1, 2, 3, 4, 5$ at $N = 500$ or 1000. We take the standard deviation of three separate runs as an estimate of the calculation error.

RESULTS AND DISCUSSION

Properties of vesicles

In this subsection, we describe the properties of vesicles without nanoparticles at $T = 0.2$. Amphiphilic molecules spontaneously form vesicles at $N > 200$ (Noguchi and Takasu, 2001a). When the initial state is random gas state with $N = 1000$, molecules aggregate into spherical or disk-shaped micelles, and they assemble and reform into vesi-

cles. Finally, all molecules belong to one vesicle. The vesicle exhibits a clear bilayer structure and is in a fluid phase. Molecules in vesicles diffuse laterally: the lateral diffusion constant is 0.0039 (±0.0004). Flip-flop motion, which is the transverse motion between inner and outer monolayers, is much slower than the lateral diffusion. The half lifetime of flip-flop motion is ~100,000 time steps.

When bilayer membrane is assumed as an elastic sheet, the free energy F of the vesicle is written as

$$F = \frac{\kappa}{2}\oint (c_1 + c_2 - c_0)^2 \, dA + \kappa_G \oint c_1 c_2 \, dA + U_0, \quad (8)$$

where κ is bending rigidity, κ_G is Gaussian bending rigidity, C_1 and C_2 are two principal curvatures, c_0 is a spontaneous curvature, and dA is an area element of the membrane (Lipowsky and Sackmann, 1995). We used the energy U instead of free-energy F, because the entropy of molecules is small in our model. It consists of translational and orientational entropies. We assume $c_0 = 0$ and $\kappa_G = 0$. The theoretical study using a simple molecular model (Suezaki and Ichinose 1995) indicates that Gaussian bending rigidity κ_G is much less than bending rigidity κ in fluid membranes. We estimated the bending rigidity κ from the fluctuation of quasi-spherical vesicles consisting of 1000 molecules (Noguchi and Takasu, 2001b). The vesicle shape is described as a series in spherical harmonics: $r(\theta, \phi) = r_0[1 + \Sigma u_{lm} Y_{lm}(\theta, \phi)]$. $r(\theta, \phi)$ is the distance between molecules and the center of mass of vesicles $\mathbf{r}_i - \mathbf{R}_G$ with spherical coordinates θ, ϕ, where $\mathbf{r}_i$ and $\mathbf{R}_G$ are the center of mass of ith molecules and the vesicle, respectively. r_0 is the radius of an equivalent surface-area sphere. We estimated $r_0 = 9.4$ (±0.2) from $\langle r \rangle = 9.17$ (±0.01) and $(\langle r \rangle - r_0)/r_0 \sim -0.1T/\kappa$. The amplitude of undulations is given by (Helfrich, 1986; Milner and Safran, 1987)

$$\langle u_{lm}^2 \rangle = \frac{T}{\kappa(l+2)(l+1)(l-1)}. \quad (9)$$

We estimate $\kappa = 1.5$ (±0.5) from u_{lm} with $l = 2$ and 3 of vesicles. u_{lm} with larger l does not fit Eq. 9 because the radius of the vesicles is not much larger than the thickness of membranes.

Figure 1 shows the size dependence of the mean energy $\langle U \rangle$ of vesicles at equilibrium. When the shape of vesicles is assumed to be a sphere, the energy $\langle U \rangle = 8\pi\kappa + U_0$ is derived from Eq. 8. U_0 is the energy to form a flat bilayer membrane from isolated amphiphilic molecules, and should be proportional to N. We obtain $\kappa = 0.6$ (±0.2) and $U_0/N = -11.21$ (±0.01) from the slope and asymptotic value at $N = \infty$ in Fig. 1, respectively. The slope of smaller vesicles becomes larger. It should be caused by some effect of smallness: the quadratic approximation of the bending energy in Eq. 8 might have error for the high curvature of small vesicles. Two estimations of κ have the same order of magnitude, and we obtain $\kappa/T \cong 5$. κ/T of phospholipid molecules is 5~100 at typical experimental condition (Lipowsky and Sackmann, 1995). The bending rigidity κ of our model is around minimum value of phospholipid. The simulated vesicles correspond to rather flexible membranes.

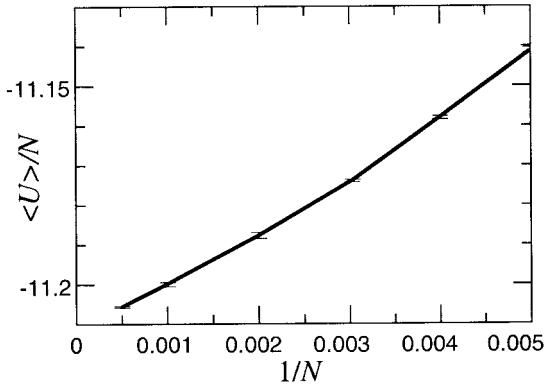

FIGURE 1 Size (N) dependence of the mean total energy $\langle U \rangle$ without nanoparticles at temperature $T = 0.2$.

U_0/NT at $T = 0.2$ are on the order of those of phospholipid molecules at typical experimental condition: $U_0/NT = -10 \sim -30$ (Tanford, 1980). The unit length σ should correspond to ~1 nm. The unit time step of our simulation corresponds to ~1 ns, when the lateral diffusion constant is assumed to correspond to that of phospholipid at 30°C, $\sim 10^{-7}$ cm^2/s (Wu, 1977).

Hydrophobic segments interact attractively via the hydrophobic potential $U_{hp}(\rho)$, and this attraction disappears at $\rho > \rho^*$ in both segments. In contrast, the Van der Waals interaction between alkyl chains remains at high density in real lipid molecules. This interaction should be significant to investigate the transition of fluid and gel phases. The improvements of the attractive potential and derivation from theories such as the density-function theory of liquid (Tarazona 1985; Denton and Ashcroft 1989) is expected in further studies.

Our present model does not represent molecules of specific chemistry. The model molecule is slightly wider or shorter than lipid molecules. The area per molecule in membranes is $2\sigma^2$. It is larger than the experimental data of lipid molecules: 50~80 Å^2 (Nagle and Tristam-Nagle, 2000). The quantitative description of lipid molecules requires the improvement of the model in comparison with the data of atomic-level MD simulations and experiments such as x-ray diffraction (Nagle and Tristam-Nagle, 2000; Lafleur et al., 1996).

Budding and fission of vesicles

In this subsection, we show the morphological change of a vesicle induced by a nanoparticle. First, we investigate stable or metastable states by a stepwise annealing simula-

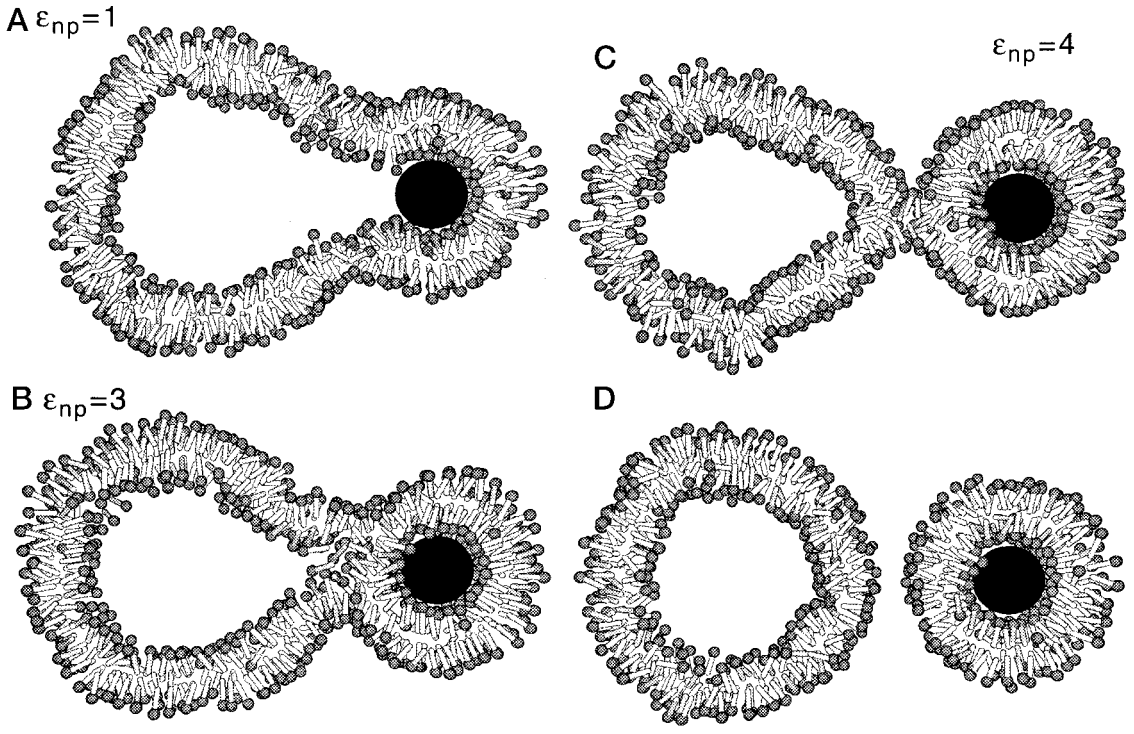

FIGURE 2 Sliced snapshots of the vesicle and the nanoparticle at $N = 2000$ and $r_{np} = 3\sigma$. Gray spheres and white cylinders represent hydrophilic and hydrophobic segments of amphiphilic molecules, respectively. A black sphere represents the nanoparticle. Molecules with $-2 \le (\mathbf{r}_i - \mathbf{R}_G)\mathbf{e}_1 < 2$ are shown from the front direction $\mathbf{e}_1$. $\mathbf{r}_i$ and $\mathbf{R}_G$ are the center of mass of ith molecule and all amphiphilic molecules, respectively. $\mathbf{e}_1$ is a the unit vector orthogonal to the direction of the nanoparticle position $\mathbf{e}_2 = (\mathbf{r}_{np} - \mathbf{R}_G)/\,\mathbf{r}_{np} - \mathbf{R}_G$. Then, $\mathbf{r}_{np}$ and $\mathbf{R}_G$ belong to the sliced region.

tion with three separate runs. We set a nanoparticle at the center of a vesicle as the initial state for the lowest ε_{np}: $\varepsilon_{np} = 0.5$ at $N = 2000$ and $\varepsilon_{np} = 0.05$ at $N = 500$ or 1000. To save computational time, we increased ε_{np} stepwise and obtained steady states. Figures 2 and 3 show the snapshots and the mean radius of gyration $\langle R_g \rangle$ of the vesicles adhering to the nanoparticle with $r_{np} = 3\sigma$ at $N = 2000$, respectively. At $\varepsilon_{np} = 0.5$, the nanoparticle adheres to the inner monolayer of the vesicle. This adhesion does not change the morphology of the vesicle much, and $\langle R_g \rangle$ at $\varepsilon_{np} = 0.5$ coincides with that of the vesicle without the nanoparticle within the calculation error. With an increase in ε_{np}, the hydrophilic segments cover larger surface of the nanoparticle, and encapsulate almost all the nanoparticle at $\varepsilon_{np} = 2$. At $\varepsilon_{np} = 1$ and 2, the vesicle exhibits pear shape, and the bilayer structure keeps well (Fig. 2 *A*). At $\varepsilon_{np} = 3$, the bilayer structure is often deformed in the pinched membrane by the side of the nanoparticle (Fig. 2 *B*). In one run, the vesicle reforms to the two connected vesicles. In the other two runs, the pear-shaped vesicles remain at $\varepsilon_{np} = 3$, and reform at $\varepsilon_{np} = 4$ (Fig. 2 *C*). The connection region exhibits cylindrical shape, and the structure is similar to the stalk intermediates in vesicle fusion (Chernomordik 1995; Noguchi and Takasu, 2001b). We call the clusters before and after morphological change as a budded state and a stalk state, respectively. The fission to two vesicles occurred in two runs at $\varepsilon_{np} = 4$ (Fig. 2 *D*), and the stalk state remains after 100,000 time steps in one run.

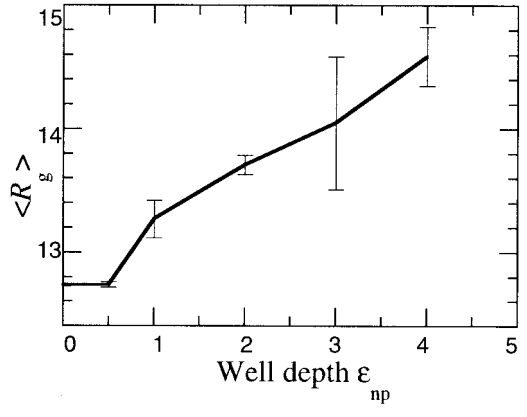

FIGURE 3 ε_{np} dependence of the mean radius of gyration $\langle R_g \rangle$ at $N = 2000$ and $r_{np} = 3\sigma$. The value of $\varepsilon_{np} = 0$ represents $\langle R_g \rangle$ of vesicles without nanoparticles. At $\varepsilon_{np} = 4$, $\langle R_g \rangle$ is only averaged over the stalk states before fission as shown in Fig. 2 *C*.

Figures 4 and 5 show the dynamics of structural change from the budded state (Fig. 2 *B*) to the stalk state (Fig. 2 *C*) at $\varepsilon_{np} = 4$. More hydrophilic segments adhere to the nanoparticle, and the bilayer structure in the pinched connection region is destabilized. The pore then opens, and the cross-

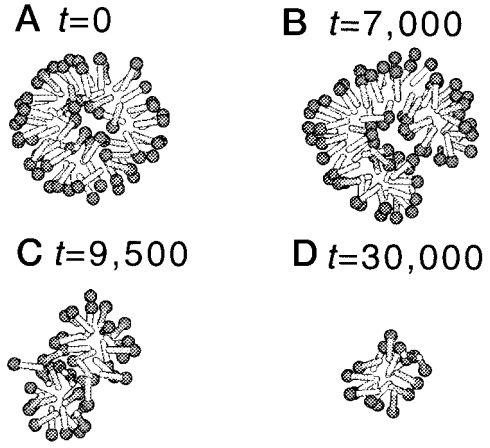

FIGURE 4 Sliced snapshots of the connection region in the structural change of the vesicle at $\varepsilon_{np} = 4$. The initial state ($t = 0$) is the pear-shaped vesicle at $\varepsilon_{np} = 3$ as shown in Fig. 2 *B*. The sliced snapshot from the front view at $t = 30{,}000$ is shown in Fig. 2 *C*. Molecules with $-1.5 \leq (\mathbf{r}_i - \mathbf{R}_0)\mathbf{e}_2 < 1.5$ are shown from the direction $\mathbf{e}_2$, where $\mathbf{R}_0 = \mathbf{r}_{np} - 8\mathbf{e}_2$ (*A*, *B*, and *C*) or $\mathbf{r}_{np} - 9\mathbf{e}_2$ (*D*).

section of the connection region becomes arc shape (Fig. 4 *B*). The arc-shaped structure separates to two stalks, and they fuse to one stalk (Fig. 4 *C*). Finally, the stalk structure is formed at 12,000 time steps (Fig. 4 *D*). U_{NP} remains decreasing for 10,000 time steps after the formation of the stalk state. Fission then occurs at 54,000 time steps. The

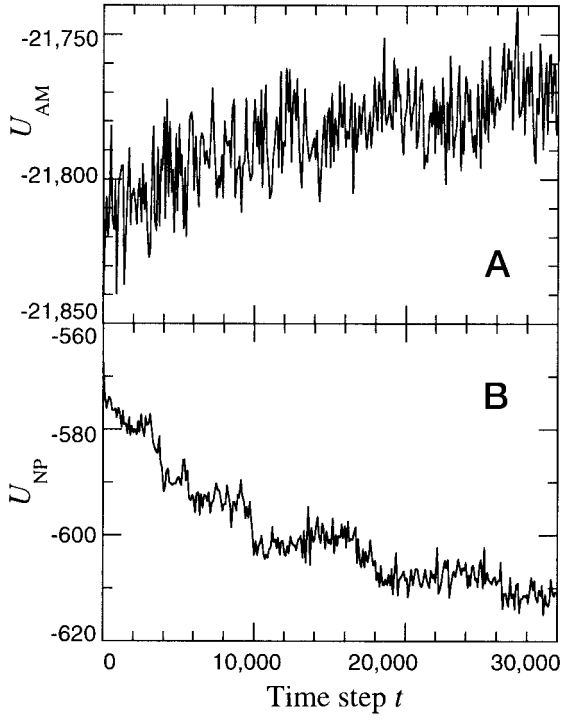

FIGURE 5 Time development of the energies U_{AM} and U_{NP} for the data shown in Fig. 4.

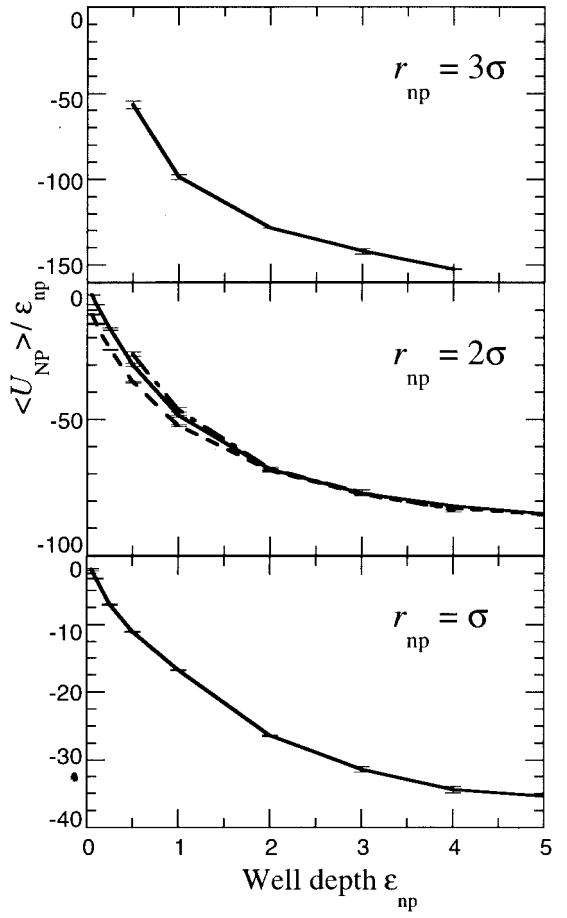

FIGURE 6 ε_{np} dependence of the mean interaction energy $\langle U_{NP} \rangle$ between amphiphilic molecules and the nanoparticle. We use $N = 2000$ at $r_{np} = 3\sigma$ and $N = 1000$ at $r_{np} = \sigma$. At $r_{np} = 2\sigma$, we change the size of vesicles: $N = 500$ (*dashed line*), $N = 1000$ (*solid line*), and $N = 2000$ (*dot-dashed* line).

stalk state is an intermediate state of fission, and has a lifetime of 40,000 time steps.

Figure 6 shows the ε_{np} dependence of the mean normalized energy $\langle U_{NP} \rangle / \varepsilon_{np}$. The decrease of $\langle U_{NP} \rangle / \varepsilon_{np}$ indicates the increase of the number of adhered molecules, and exhibits no abrupt transition. The budding induced by a nanoparticle is continuous morphological change. We define the number of adhered molecules N_{adh} as that of the molecules, which hydrophilic segment is closer than $r_{np} + r_{am} + 0.7\sigma$ to the nanoparticle. When $N = 2000$ and $r_{np} = 3\sigma$, the normalized energy per an adhered molecule $\langle U_{NP} \rangle / \langle N_{adh} \rangle \varepsilon_{np} = -0.89$ (± 0.05) and -0.97 (± 0.01) at $\varepsilon_{np} = 0.5$ and 4, respectively. It exhibits weak ε_{np} dependence within 10% of value.

Figure 7 shows the energy differences $\langle \Delta U_{AM} \rangle$, $\langle \Delta U_{REP} \rangle$, and $\langle \Delta U_{HP} \rangle$, the energies of vesicles minus those of vesicles without nanoparticles. In the annealing simulation, $\langle U_{AM} \rangle$ increases with an increase in ε_{np}. This energy increase is mainly caused by repulsion between adhered molecules. On

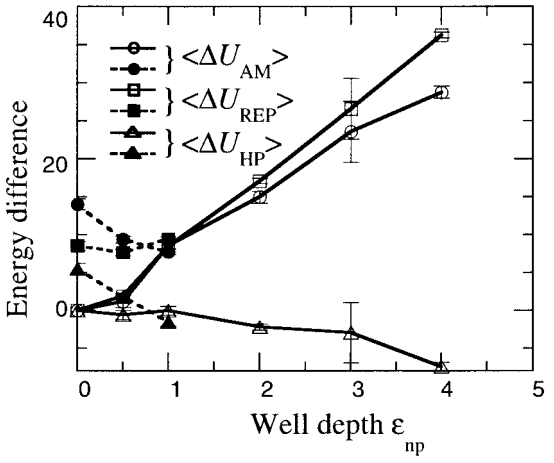

FIGURE 7 ε_{np} dependence of the mean interaction energies between amphiphilic molecules at $N = 2000$ and $r_{np} = 3\sigma$. The energies minus those of vesicles without nanoparticles are shown: $\Delta U_{AM} = U_{AM} - U^{v}_{AM}$, where U^{v}_{AM} is U_{AM} of vesicles without nanoparticles: $U^{v}_{AM} = -22411.2$ (± 0.4). ΔU_{REP} and ΔU_{HP} are the energy differences for the repulsive and hydrophobic potentials, respectively. $U^{v}_{REP} = 389.4$ (± 0.2) and $U^{v}_{HP} = -22800.6$ (± 0.4). Open symbols and solid lines represent the results of annealing simulation. Closed symbols with dashed lines represent the results starting the stalk states as shown in Fig. 2 *C*. The values at $\varepsilon_{np} = 0$ represent those of vesicles without nanoparticles.

the surface of the nanoparticle, the molecules are in order with high density, and $\langle \Delta U_{HP} \rangle$ decreases. In the simulation starting with stalk states, the stalk structure remains even without the nanoparticle. Thus, the budded and stalk states are in the local minima of the free-energy landscape. The energies of both states equal at $\varepsilon_{np} \cong 1$. At larger ε_{np}, the stalk state is more stable. At smaller ε_{np}, the budded state or the vesicle with the isolated nanoparticle is more stable.

When the radius of nanoparticle r_{np} is σ or 2σ, the stalk state is not observed even at $\varepsilon_{np} = 5$. The vesicles exhibit similar structures as shown in Fig. 2, *A* and *B*. U_{NP} is dependent slightly on N at $r_{np} = 2\sigma$ as shown in Fig. 6. At $N = 500$, the budded part of vesicle encapsulating the nanoparticle is larger than the other part at $\varepsilon_{np} = 5$. Thus, the number of adhered molecules depends slightly on the morphology of vesicles.

Next, we describe the adhesion of a nanoparticle from the outside of a vesicle at $N = 2000$, $r_{np} = 3\sigma$, and $\varepsilon_{np} = 4$. We set the nanoparticle outside of the vesicle at initial states. Figures 8 and 9 show the sequential snapshots and the time development of U and R_g of the adhesion process. The nanoparticle contacts the outer monolayer of the vesicle at 3600 time steps. First, the nanoparticle begins to bud to the inside of the vesicle (Fig. 8 *A*), and R_g decreases. Because the membrane shows acute angles by the sides of the bud, the outer monolayers reform to bilayer structure there (see upper side in Fig. 8 *A*). The membrane then encapsulates the nanoparticle (Fig. 8 *B*). To reduce the connection region, the encapsulated nanoparticle gradually moves to the outside of the vesicle (Fig. 8 *C*), and R_g increases. Finally, the vesicle changes to the stalk state (Fig. 8 *D*). The pathway of for-

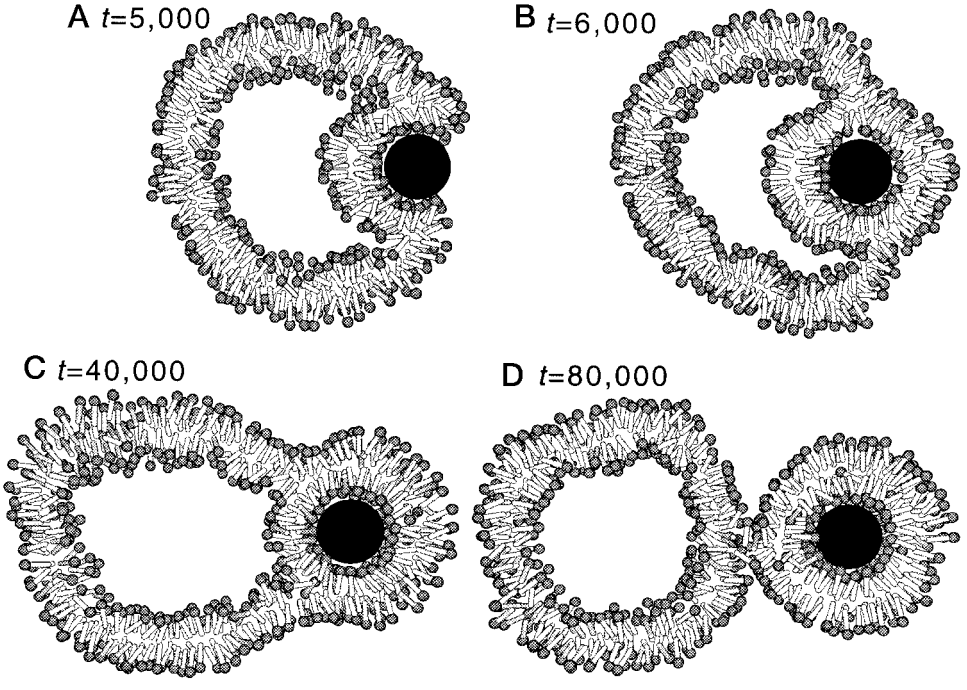

FIGURE 8 Sequential snapshots of adhesion process of the nanoparticle from the outside of a vesicle at $r_{np} = 3\sigma$, $\varepsilon_{np} = 4$, and $N = 2000$. Snapshots depict the same as Fig. 2.

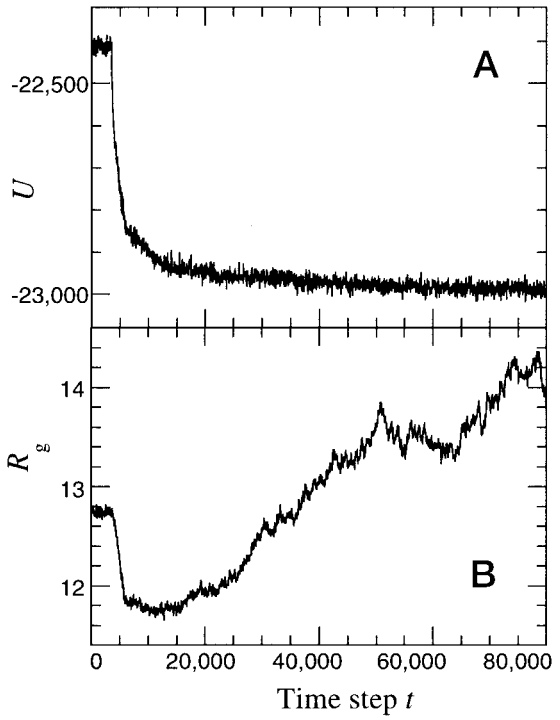

FIGURE 9 Time development of the total energy U and the radius of gyration R_g for the data shown in Fig. 8.

mation of the stalk structure is the same as in Fig. 4. We observed these morphological changes in three separate runs. The fission is then observed in two runs, and the stalk states remain after 130,000 time steps in the other run. Thus, the final structures are almost independent of initial states.

The simulated vesicles correspond to diameters of <25 nm. The usual budding events occur on lipid and biological vesicles >100 nm in diameter. However, the number of adhered molecules is almost independent of the size of vesicles, and the structures around the nanoparticle are slightly modified. When a larger vesicle is used, the vesicle adhered by the nanoparticle from outside would bud to the inside of the vesicle. Volume of the simulated vesicles is not fixed, because our model does not take into account explicit solvent molecules. Under volume constraint, a small spherical vesicle cannot bud. The ellipsoidal vesicles or sufficiently large vesicles are needed to obtain budding. In the experiment of adhesion of Latex spheres (Dietrich et al. 1997), the volume of the vesicles changes during adhesion. It is caused by water flow through pores on a membrane. They also observed expulsion and recapture after ingestion using multi-lamellar vesicles.

We only observed the stalk formation and fission at $r_{np} = 3\sigma$. The high curvature of connection region at $r_{np} = 3\sigma$ should promote the transition to stalk structure. Larger nanoparticles with $r_{np} > 3\sigma$ may induce the stalk formation and fission well. In our simulation, the adhesion energy per molecule (per area) for the stalk formation is $\varepsilon_{np}/T = 20$ (4×10^{-2} J/m^2), and seems too large. However, this energy should decrease for larger particles. When membrane tension is generated by morphological change to a pear-shape vesicle, the tension should reduce the energy for membrane deformation in stalk formation.

In our simulation, the membrane curves toward the nanoparticle. In contrast, coat proteins (Schekman and Orci, 1998) and anchored polymers (Tsafrir et al., 2001) curve membrane toward the opposite side. It is interesting to examine this type of induction process into budding and fission, and to compare it with the induction by the nanoparticle.

Fusion process promoted by nanoparticle

In this subsection, we show that the fusion of vesicles is promoted by a nanoparticle. In our previous paper (Noguchi and Takasu, 2001b), we have clarified the two pathways of spontaneous fusion of two vesicles at $T = 0.2$ and 0.5. At higher temperature $T = 0.5$, the contacted vesicles form a neck-like structure that only connects outer monolayers (see Fig. 10 *A*). This structure corresponds to a stalk intermediate in the stalk model (Chernomordik et al., 1995). The cross-section shape of the stalk often changes from circle to ellipse by thermal fluctuation. When a small pore connecting the inside and outside of a vesicle opens by the side of the elliptic stalk, the stalk bends around the pore, and the fusion pore connecting the insides of vesicles opens. At $T = 0.2$, the vesicles are stable, and the contacted vesicles do not form the stalk intermediate. We used the stalk intermediate at $T = 0.5$ as the initial states, and investigated the pore-opening process. Some vesicles fuse through the pathway predicted by modified stalk model (Siegel, 1993): the inner monolayers contact inside the radially expanded stalk, and the fusion pore opens. The quenching from $T = 0.5$ to $T = 0.2$ have promotion effect on the pore opening. The stalks, which do not fuse in 10,000 time steps, are stabilized, and remain after 100,000 time steps. We used these stabilized stalk intermediate and the nanoparticle with $r_{np} = \sigma$ as the initial states.

Figures 10 and 11 show the sequential snapshots and the time development of the energies U_{AM} and U_{NP} of the fusion process at well depth $\varepsilon_{np} = 1$. First, the nanoparticle adheres to the surface of a vesicle (Fig. 10 *A*). The nanoparticle diffuses on the surface, and reaches the side of the stalk (Fig. 10 *B*). The energy U_{NP} decreases from -10 to -20 (Fig. 11 *B*) because the nanoparticle contacts more amphiphilic molecules of both vesicles. The stalk bends around the nanoparticle, and the pore opens on a vesicle (Fig. 10, *C* and *G*). The pore then opens on the other vesicle (Fig. 10 *D*), and the fusion pore that connects the insides of the vesicles is formed (Fig. 10 *E*). The vesicle exhibits pear shape, and the nanoparticle contacts the amphiphilic molecules on an equatorial line as shown in Fig. 10 *E*. This structure is metastable and remains until 24,000 time steps.

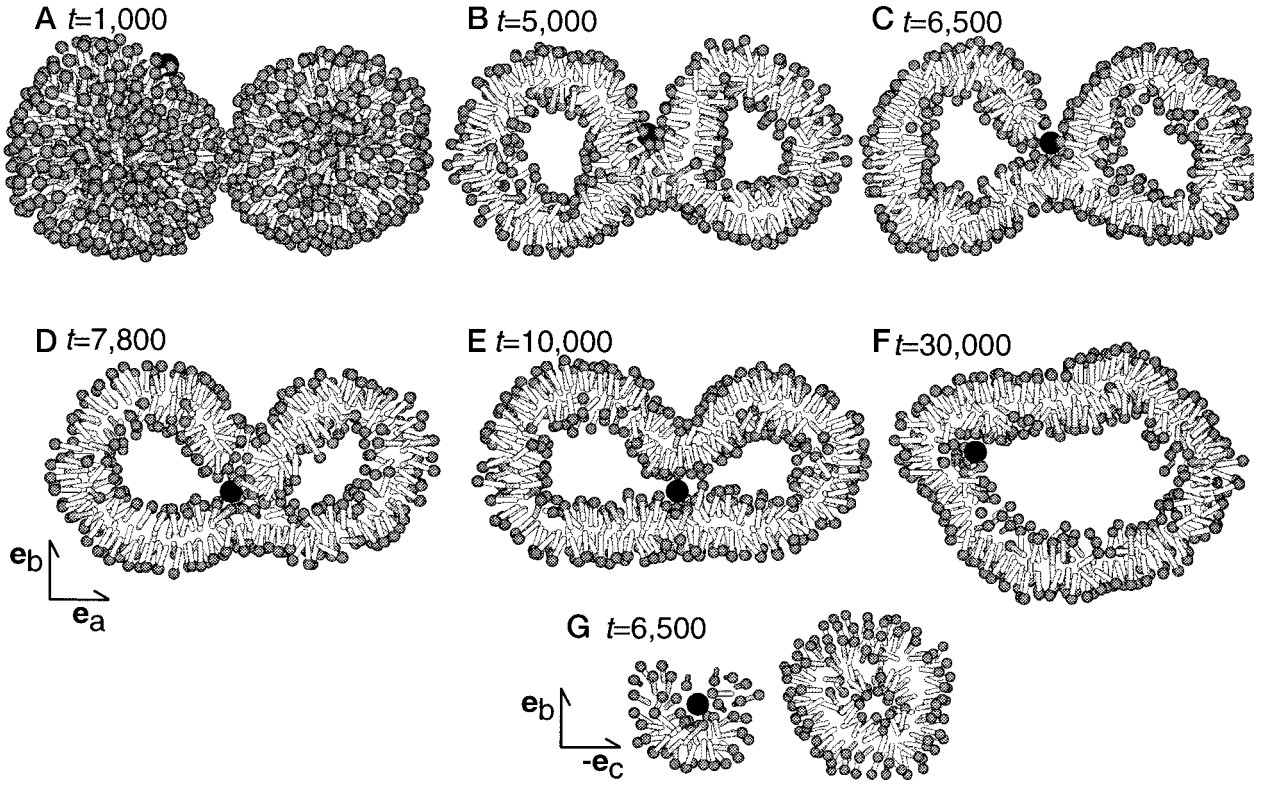

FIGURE 10 Sequential snapshots of fusion process promoted by the nanoparticle at $r_{np} = \sigma$, $\varepsilon_{np} = 1$, and $N = 1000$. The snapshots are viewed from $\mathbf{e}_c$ (*A–F*) or $\mathbf{e}_a$ (*G*) direction. $\mathbf{e}_a$ is the eigenvector of the largest eigenvalue of the moment tensor of inertia. $\mathbf{e}_b = (\mathbf{r}_{np} - \mathbf{R}_G)/\,\mathbf{r}_{np} - \mathbf{R}_G$ and $\mathbf{e}_c = \mathbf{e}_a \times \mathbf{e}_b$. (*A*) All molecules are shown. (*B–F*) Molecules with $-2 \le (\mathbf{r}_i - \mathbf{R}_G)\,\mathbf{e}_c < 2$ are shown. (*G*) Molecules with $-1.5 \le (\mathbf{r}_i - \mathbf{r}_{np})\,\mathbf{e}_a < 1.5$ (*left*) or with $-4.5 \le (\mathbf{r}_i - \mathbf{r}_{np})\,\mathbf{e}_a < -1.5$ (*right*) are shown.

Finally, the part of the membrane is detached from the nanoparticle, and the vesicle becomes spherical shape (Fig. 10 *F*). We obtain this stalk-bending pathway in four separate runs. At $\varepsilon_{np} = 0.5$, the vesicles fuse through the same pathway in one run, and the vesicles remain in the stalk intermediate after 100,000 time steps in three runs. At $\varepsilon_{np} = 2$, the vesicles fuse in four separate runs. However, the pear-shaped vesicle (Fig. 10 *E*) remains after 100,000 time steps in all runs. At $\varepsilon_{np} = 2.5$, the nanoparticle induces the budding of a contacted vesicle through similar process as shown in Fig. 8 in two runs, and the pear-shaped vesicle is formed in the other two runs.

These results indicate that the nanoparticle clearly promotes the stalk-bending process. The nanoparticle bends the stalk. The vesicle surface near the arc-shaped stalk becomes unstable by the high bending curvature, and a pore opens. The adhesion force with the appropriate strength is needed for the fusion promotion. The nanoparticle with larger ε_{np} induces budding on the contacted vesicle surface. The nanoparticle with smaller ε_{np} does not change the vesicle states.

Some fusion proteins may promote the stalk-bending process. We used the simple spherical nanoparticle containing no hydrophobic part. The protein structures are more complex, and contain hydrophobic domains. The way of

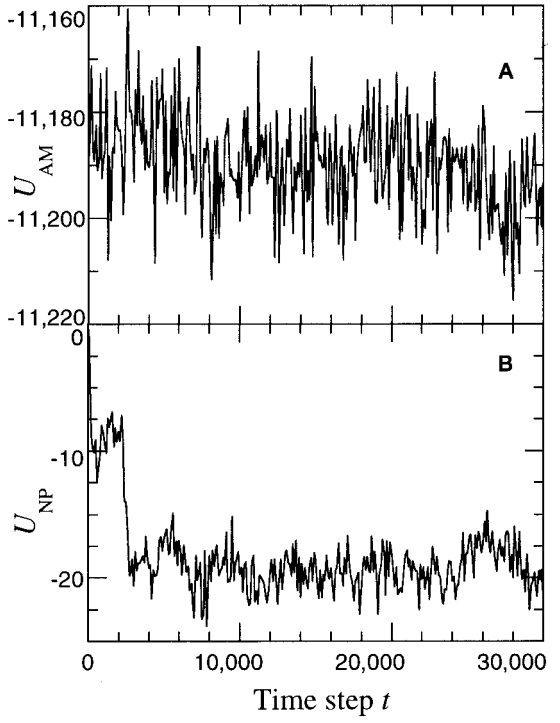

FIGURE 11 Time development of the energies U_{AM} and U_{NP} for the data shown in Fig. 10.

promotion by proteins may be slightly modified. Though the stalk bends around the nanoparticle in our simulation, the protein may bend to the opposite side. The protein then exists on the outside surface of the vesicle after fusion, and can promote the fusion with another vesicle again. The hydrophobic segments of protein might mediate the pore opening on a vesicle by the side of the stalk. Though the pore connecting the inside and outside of a vesicle is small and opens within short time, ~ 1 μs, some solvent molecules can flow between the inside and outside of a vesicle through the pore. In many biological fusions, this flow should not be acceptable, and may be avoided by the shield of the protein. The nanoparticle almost covers the pore in our simulation.

In our simulation, the high bending curvature of small vesicles with a diameter of 20 nm mediates fusion, and the fusion rate of larger vesicles is slower. The local curvature of membranes is important in the fusion mediated by proteins such as hemagglutinin. At the beginning of fusion, the bending structure of a membrane protruding toward the other membrane, called dimple or microprotrusion, is observed by quick-freezing electron microscopy (Chandler and Heuser, 1980; Ornberg and Reese, 1981; Kanaseki et al., 1997). Its diameter is 10–20 nm. This dimple largely reduces the energy to create the stalk (Kuzmin et al., 2001). Thus, we can interpret that the dimple is mimicked by the vesicle in our simulation. The obtained fusion pathways may exist in large vesicles with μm scale.

CONCLUSIONS

We have shown that nanoparticles induce the structural changes of vesicles: budding, stalk formation, and fission. We have clarified that a stalk state is fission intermediate between budded and separated states. The budded vesicle changes to the stalk state through pore opening at the connection region.

We have also shown that the nanoparticle promotes the fusion process from the stalk intermediate to the fusion-pore opening. The bound nanoparticle bends the stalk and induces the pore that connects the inside and outside of a vesicle. Some fusion proteins may use the same promotion method.

We used the simple model with the absence of solvent molecules and hydrodynamic interactions. This absence should modify the dynamics quantitatively. Particularly, it is biologically important whether water molecules flow through the pores opened on membranes in fission and fusion processes. When the budding needs volume change, the budding is accompanied with pore opening and water flow through it. The further studies using MD or DPD simulations are required to clarify these. We changed adhesion strength only by ε_{np}. It depends on the surface density of ligands and receptors for adhesion caused by specific ligand binding. In low receptor concentration, the adhesion couples the lateral diffusion of receptors on a vesicle (Boulbitch et al., 2001). It is interesting to examine this effect on structural changes. We hope that further experimental studies will reveal fission and fusion promotion processes in real systems.

Note: After submitting the present paper, we received the preprint about membrane fusion (Müller et al., 2002) from Prof. M. Schick. They observed similar fusion behavior to stalk-bending process using a lattice Monte Carlo simulation. They used a different model from ours, and its amphiphilic molecules are flexible. This may suggest that stalk-bending process occurs in membrane fusion of various amphiphilic molecules.

This work was supported in part by a grant-in-aid for Scientific Research from the Ministry of Education, Culture, Sports, Science, and Technology of Japan.

REFERENCES

Allan, B. B., and W. E. Balch. 1999. Protein sorting by directed maturation of Golgi compartments. *Science.* 285:63–66.

Allen, M. P., and D. J. Tildesley. 1987. Computer Simulation of Liquids. Clarendon Press, Oxford, U.K. 91–92.

Angelova, M. I., and I. Tsoneva. 1999. Interactions of DNA with giant liposomes. *Chem. Phys. Lipids.* 101:123–137.

Bernardes, A. T. 1996. Monte Carlo simulation of vesicle self-organisation. *J. Phys. II (France).* 6:169–174.

Boulbitch, A., Z. Guttenberg, and E. Sackmann. 2001. Kinetics of membrane adhesion mediated by ligand–receptor interaction studied with a biomimetic system. *Biophys. J.* 81:2743–2751.

Chandler, D. E., and J. E. Heuser. 1980. Arrest of membrane fusion events in mast cells by quick-freezing. *J. Cell Biol.* 86:666–674.

Chen, C.-M., P. G. Higgs, and F. C. MacKintosh. 1997. Theory of fission for two-component lipid vesicles. *Phys. Rev. Lett.* 79:1579–1582.

Chenevier, P., B. Veyret, D. Roux, and N. Henry-Toulmé. 2000. Interaction of cationic colloids at the surface of J774 cells: a kinetic analysis. *Biophys. J.* 79:1298–1309.

Chernomordik, L., M. M. Kozlov, and J. Zimmerberg. 1995. Lipids in biological membrane fusion. *J. Membr. Biol.* 146:1–14.

Denton, A. R., and N. W. Ashcroft. 1989. Modified weight-density-functional theory of nonuniform classical liquids. *Phys. Rev. A.* 39: 4701–4708.

Dietrich, C., M. Angelova, and B. Pouligny. 1997. Adhesion of Latex spheres to giant phospholipid vesicles: statics and dynamics. *J. Phys. II (France).* 7:1651–1682.

Goetz, R., G. Gompper, and R. Lipowsky. 1999. Mobility and elasticity of self-assembled membranes. *Phys. Rev. Lett.* 82:221–224.

Groot, R. D., T. J. Madden, and D. J. Tildesley. 1999. On the role of hydrodynamic interactions in block copolymer microphase separation. *J. Chem. Phys.* 110:9739–9749.

Groot, R. D., and K. L. Rabone. 2001. Mesoscopic simulation of cell membrane damage, morphology change and rupture by nonionic surfactants. *Biophys. J.* 81:725–736.

Helfrich, W. 1986. Size distributions of vesicles: the role of the effective rigidity of membranes. *J. Phys. (France).* 47:321–329.

Hotani, H., F. Nomura, and Y. Suzuki. 1999. Giant liposomes: from membrane dynamics to cell morphogenesis. *Curr. Opin. Coll. Interface Sci.* 4:358–368.

Huebner, S., B. J. Battersby, R. Grimm, and G. Cevc. 1999. Lipid-DNA complex formation: reorganization and rupture of lipid vesicles in the

presence of DNA as observed by cryoelectron microscopy. *Biophys. J.* 76:3158–3166.

Jahn, R., and T. C. Südhof. 1999. Membrane fusion and exocytosis. *Annu. Rev. Biochem.* 68:863–911.

Kanaseki, T., K. Kawasaki, M. Murata, Y. Ikeuchi, and S.-i. Ohnishi. 1997. Structure features of membrane fusion between influenza virus and liposome as revealed by quick-freezing electron microscopy. *J. Cell Biol.* 137:1041–1056.

Kawakatsu, T. 1997. Effects of changes in the chain conformation on the kinetics of order–disorder transitions in block copolymer melts. *Phys. Rev. E.* 56:3240–3250.

Kumar, P. B. S., G. Gompper, and R. Lipowsky. 2001. Budding dynamics of multicomponent membranes. *Phys. Rev. Lett.* 86:3911–3914.

Kuzmin, P. I., J. Zimmerberg, Y. A. Chizmadzhev, and F. S. Cohen. 2001. A quantitative model for membrane fusion based on low-energy intermediates. *Proc. Natl. Acad. Sci. U.S.A.* 98:7235–7240.

Lafleur, M., M. Bloom, E. F. Eikenberry, S. M. Gruner, Y. Han, and P. R. Cullis. 1996. Correlation between lipid plane curvature and lipid chain order. *Biophys. J.* 70:2747–2757.

Li, X.-j. and M. Schick. 2000. Distribution of lipids in nonlamellar phases of their mixtures. *J. Chem. Phys.* 112:6063–6072.

Lindahl, E., and O. Edholm. 2000. Mesoscopic undulations and thickness fluctuations in lipid bilayers from molecular dynamics simulations. *Biophys. J.* 79:426–433.

Lipowsky, R., and E. Sackmann, editors. 1995. Structure and Dynamics of Membranes. *In* Handbook of Biological Physics, Elsevier, Amsterdam, The Netherlands.

Maurits, N. M., A. V. Zvelindovsky, G. J. A. Sevink, B. A. C. van Vlimmeren, and J. G. E. M. Fraaije. 1998. Hydrodynamic effects in three-dimensional microphase separation of block copolymers: dynamic mean-field density functional approach. *J. Chem. Phys.* 108: 9150–9154.

Milner, S. T., and S. A. Safran. 1987. Dynamical fluctuations of droplet microemulsions and vesicles. *Phys. Rev. A.* 36:4371–4379.

Müller, M., K. Katsov, and M. Shick. 2002. New mechanism of membrane fusion. *J. Chem Phys.* 116:2342–2345.

Nagle, J. F., and S. Tristram-Nagle. 2000. Lipid bilayer structure. *Curr. Opin. Struct. Biol.* 10:474–480.

Netz, R. R., and M. Schick. 1996. Pore formation and rupture in fluid bilayers. *Phys. Rev. E.* 53:3875–3885.

Noguchi, H., and M. Takasu. 2001a. Self-assembly of amphiphiles into vesicles: a Brownian dynamics simulation. *Phys. Rev. E.* 64:041913 (7 pages).

Noguchi, H., and M. Takasu. 2001b. Fusion pathways of vesicles: a Brownian dynamics simulation. *J. Chem. Phys.* 115:9547–9551.

Noguchi, H., and M. Takasu. 2002. Structural changes of pulled vesicles: a Brownian dynamics simulation. *Phys. Rev. E.* 65. In press.

Ohta-Iino, S., M. Pasenkiewicz-Gierula, Y. Takaoka, H. Miyagawa, K. Kitamura, and A. Kusumi. 2001. Fast lipid disorientation at the onset of membrane fusion revealed by molecular dynamics simulations. *Biophys. J.* 81:217–224.

Ornberg, R. L., and T. S. Reese. 1981. Beginning of exocytosis captured by rapid-freezing of limulus amebocytes. *J. Cell Biol.* 90:40–54.

Pastor, R. W. 1994. Molecular dynamics and Monte Carlo simulations of lipid bilayers. *Curr. Opin. Struct. Biol.* 4:486–492.

Saiz, L., and M. L. Klein. 2001. Structure properties of a highly polyunsaturated lipid bilayer from molecular dynamics simulations. *Biophys. J.* 81:204–216.

Schekman, R., and L. Orci. 1998. Coat proteins and vesicle budding. *Science.* 271:1526–1533.

Siegel, D. P. 1993. Energetics of intermediates in membrane fusion: comparison of stalk and inverted micellar intermediate mechanisms. *Biophys. J.* 65:2124–2140.

Suezaki, Y., and H. Ichinose. 1995. A theory on the bending moduli of thin membranes by the use of a simple molecular model. *J. Phys. I (France).* 5:1469–1480.

Tanford, C. 1980. The Hydrophobic Effect: Formation of Micelles and Biological Membranes. 2nd ed. John Wiley and Sons, New York.

Tarazona, P. 1985. Free-energy density functional for hard spheres. *Phys. Rev. A.* 31:2672–2679.

Tieleman, D. P., S. J. Marrink, and H. J. C. Berendsen. 1997. A computer perspective of membranes: molecular dynamics studies of lipid bilayer systems. *Biochim. Biophys. Acta.* 1331:235–270.

Tsafrir, I., D. Sagi, T. Arzi, M.-A. Guedeau-Boudeville, V. Frette, D. Kandel, and J. Stavans. 2001. Pearling instabilities of membrane tubes with anchored polymers. *Phys. Rev. Lett.* 86:1138–1141.

van Vlimmeren, B. A. C., N. M. Maurits, A. V. Zvelindovsky, G. J. A. Sevink, and J. G. E. M. Fraaije. 1999. Simulation of 3D mesoscale structure formation in concentrated aqueous solution of the triblock polymer surfactants (ethylene oxide)$_{13}$(propylene oxide)$_{30}$(ethylene oxide)$_{13}$ and (propylene oxide)$_{19}$(ethylene oxide)$_{33}$(propylene oxide)$_{19}$. Application of dynamic mean-field density functional theory. *Macromolecules.* 32:646–656.

Woodle, M. C., and P. Scaria 2001. Cationic liposomes and nucleic acids. *Curr. Opin. Coll. Interface Sci.* 6:78–84.

Wu, E.-S., K. Jacobson, and D. Papahadjopoulos. 1977. Lateral diffusion in phospholipid multibilayers measured by fluorescence recovery after photobleaching. *Biochemistry.* 16:3936–3942.

Yamamoto, S., Y. Maruyama, and S.-a. Hyodo. 2002. Dissipative particle dynamics study of spontaneous vesicle formation of amphiphilic molecules. *J. Chem Phys.* 116:5842–5849.